TUNABLE BROADBAND ALL-DIELECTRIC PERFECT ABSORBER BASED ON PHASE CHANGE MATERIAL

Zongren[1] Zhang and Tao Wei[2]

[1]Mary Institute and Country Day School, St. Louis. USA
[2]Suzhou University of Technology, Suzhou, China

ABSTRACT

This work reported a polarization-independent, all-dielectric perfect absorber based on phase-change material. Broadband (in the wavelength range of 400-1000 nm) absorption of higher than 90% has been realized in our designed absorber. Moreover, absorption bandwidth and absorptivity can be tuned via structural parameters (such as the period, height and radius of nanopillars, the thicknesses of TiO2 and bottom GeTe films) and phase-change process. The underlying physical mechanism of the absorber is analyzed in detail. The proposed all-dielectric perfect absorber has potential applications in solar energy harvesting.

KEYWORDS

Perfect absorber, amorphous state, crystalline state, absorption spectra

1. INTRODUCTION

Recent years, green energy sources have attracted much attention owing to the current energy crisis problems. Solar energy, as a promising green energy source, has particularly been attracting attentions for its applications in thermal energy, power generation or chemical reactions1. However, the efficient extraction of solar energy and the conversion into other forms of usable energy still face huge challenges. Solar absorber has the ability to efficiently address the challenges. Therefore, to design a perfect solar absorber with high efficiency ultra-broadband is of great significance.

Metamaterial is an artificial composite, which possesses significant electromagnetic properties such as the special design and arbitrary control of electromagnetic wave propagation[2]. It has potential applications such as superlenses, negative refraction, optical cloaking and so on[3-5]. Since Landy et al.[6] reported a perfect metamaterial absorber in 2008, perfect absorber based on metamaterials has been extensively investigated by researchers, which provides new idea to address the above-mentioned challenges. So far, the development of perfect absorbers ranges from single-band absorption[7, 8], multi-band absorption[9, 10] to even broadband absorption[11-14] Among others, broadband absorber has been extensively investigated for solar cells, thermophotoelectric, thermal radiation, infrared imaging, etc[1, 13, 15]. For instance, Deng et al. Reported a SiO2/Cr/SiO2 three-layer absorber in which absorption of higher than 90% in a spectral range of 400-1400 nm had been realized[16]. Luo et al. proposed a broadband absorber with the absorption of 90% in the wavelength of 400-700 nm and polarization independent[17] . Qi et al. reported an ultra-broadband absorber based on all-metal and connected cylindrical holes[18]. In this structure, more than 90% absorptivity can be achieved under normal incidence, ranging 300 to 1260 nm. However, the reported perfect absorbers cannot achieve bandwidth tunability.

Besides, the designed structures involve metal material, which is readily eroded by air environment and thus have limitation in solar energy harvesting.

Therefore, all-dielectric perfect absorber without metal material has more promising respect in solar energy harvesting. Unfortunately, all-dielectric absorbers are rarely reported for the solar energy field. Moreover, all-dielectric absorbers with broadband and tunable absorption have not yet reported up to now. In this case, an all-dielectric perfect absorber possessing broadband and tunability is reported in this work.

In order to achieve tunable bandwidth, phase change material is utilized in our absorber. Phase change material (such as GeTe) has been widely used in optical and electronic memories due to its large optical or resistance contrast between amorphous and crystalline states at optical or electric stimulas[19]. Tunable metamaterials based on phase change materials have also been extensively investigated for optical sensing[20], thermal emitter[21] and so on[22-24]. Thereby, an all dielectric absorber based on phase change material is proposed in our work for solar energy harvesting. The optical absorption characteristics of our designed absorber are theoretically investigated in detail. The influence of structural parameters on absorption performance is elucidated. The physical mechanism of perfect absorber is finally analyzed.

2. STRUCTURAL DESIGN AND SIMULATION

To achieve broadband perfect absorption, all-dielectric perfect absorber is designed and the schematic diagram is shown in Fig.1. Fig.1a is the stereogram view of perfect absorber. It is worth mentioning that absorber on horizontal direction (x-y plane) consists of infinite numbers of GeTe nanopillars and only some of unit cells are illustrated. The nanopillars are periodically in order and the related parameters are marked in Fig.1b (side view) and Fig.1c (top view). Here, the period of structural unit is marked as p; the radius of GeTe nanopillar is marked as r_{GeTe}; the height is marked as h_{GeTe}; the thicknesses of TiO_2 and GeTe thin film are marked as d_{TiO2} and d_{GeTe}, respectively.

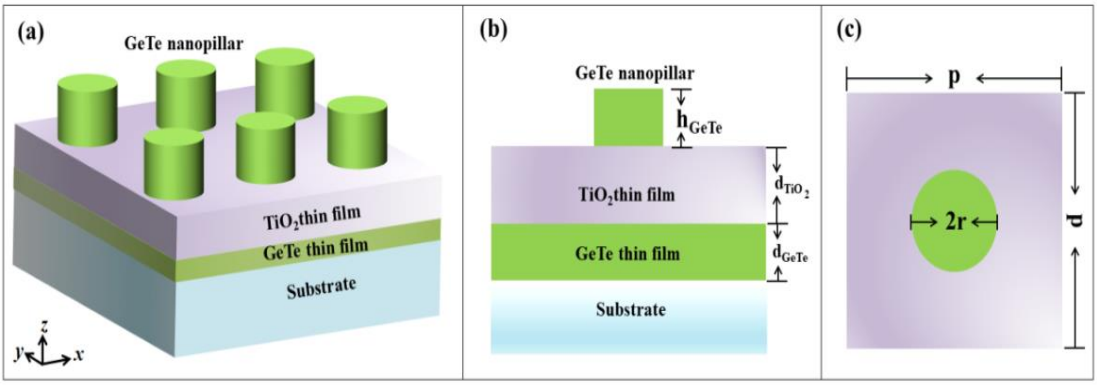

Fig.1 The structure design of the all-dielectric perfect absorber：(a) Stereogram view; (b) side view and (c) top view

In our designed structure, GeTe thin film is selected owing to large optical contrast (that is, the large difference of refractive index and extinction coefficient) between amorphous and crystalline state, which is beneficial for the realization of tunable absorption via the phase change process[25]. TiO_2 thin film is used as transparent dielectric layer owing to the high transmittance in the wide

wavelength range. Fig. 2 shows the optical constants of TiO_2 and GeTe thin films,which is obtained from related reference[26-28].

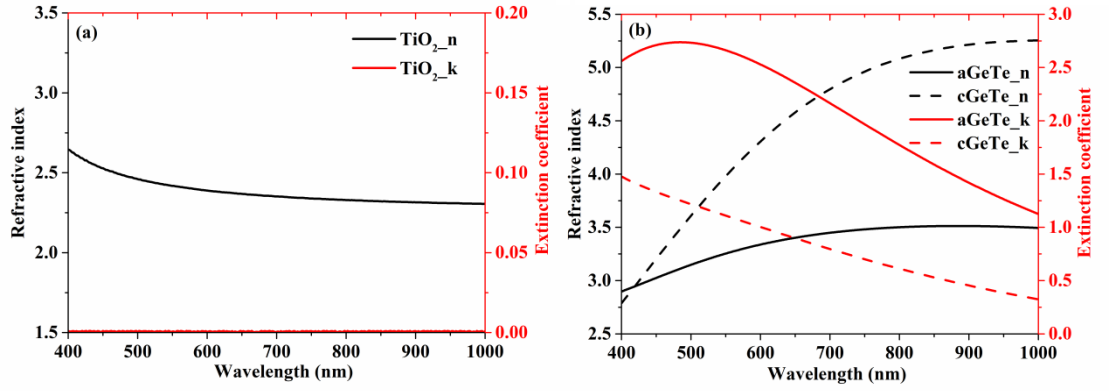

Fig.2 Optical constants (n and k) of (a) TiO_2; (b) amorphous and crystalline GeTe thin films (labeled as aGeTe and cGeTe), which is obtained from Ref.[26-28].

According to the proposed structure and optical constants of TiO2 and GeTe thin films, absorption spectra in the wavelength range of 400~1600 nm are simulated by finite element method (FEM)under p-polarized (TM, the direction of the incident electric field is along the x axis) and s-polarized (TE, the direction of the incident electric field is along the y axis) incident light. The normal incidence direction of excitation light is the normal direction of the structural plane, that is, the z direction. Periodic boundary conditions are utilized to approximate an infinite nanopillars in the x and y directions, and perfect matching layers are set in the z direction. The perfect absorber is operated in air.

3. RESULTS AND DISCUSSION

Fig.3 shows the absorption spectra of the designed absorbers at different polarizations, where the period, radius and height of amorphous GeTe nanopillar are 350 nm, 80 nm and 150 nm, respectively. The thicknesses of middle TiO2 layer and bottom amorphous GeTe thin film are 40 nm and 200 nm, respectively. It can be found that two different polarizations coincide well with each other, clearly demonstrating the polarization-independent performance of our designed absorber. At the same time, the designed absorber possesses high absorptivity (>90%) in the broad wavelength range of 400~1000 nm. Therefore, the proposed all-dielectric absorber can achieve broadband perfect absorption with the bandwidth of 600 nm.

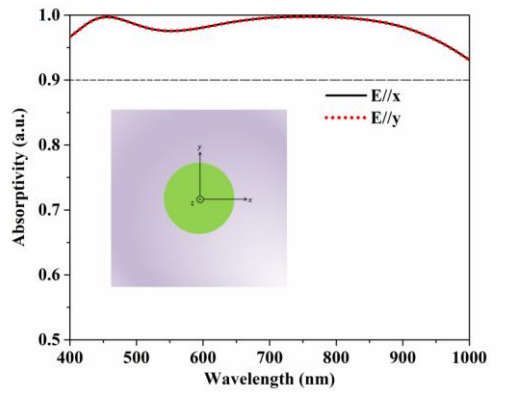

Fig.3 Absorption spectra of the designed absorbers at different polarizations

In order tounderstand the underlying physical mechanism of the broadband performance, Fig.4 displays the electromagnetic field distributions of the proposed absorbers at the wavelengths of 455 nm and 755 nm, respectively. It is worth mentioning that the choice of 455 nm and 755 nm wavelengths is due to the maximum absorption peaks as shown in Fig.3. It is obvious from Figs.4a and 4c that at the wavelength of 455 nm, both the electric and magnetic fields are concentrated mainly around the edge of the amorphous GeTe nanopillar in the air layer. Besides, magnetic field is the strongest between TiO2 and amorphous GeTe thin films, which is consistent with the features of Fabry–Pérot(FP) resonance29. At the wavelength of 755 nm, as shown in Figs.4b and 4d, the electric and magnetic fields are strongest at the top and bottom edges of amorphous GeTe nanopillar, causing electric and magnetic resonances around the GeTe nanopillar. In addition, the magnetic field is also focused inside the TiO2 thin films, resulting in the magnetic resonance inside the TiO2 film. Therefore, the broadband absorption can be achieved by tailoring the modes of electric and magnetic resonances.

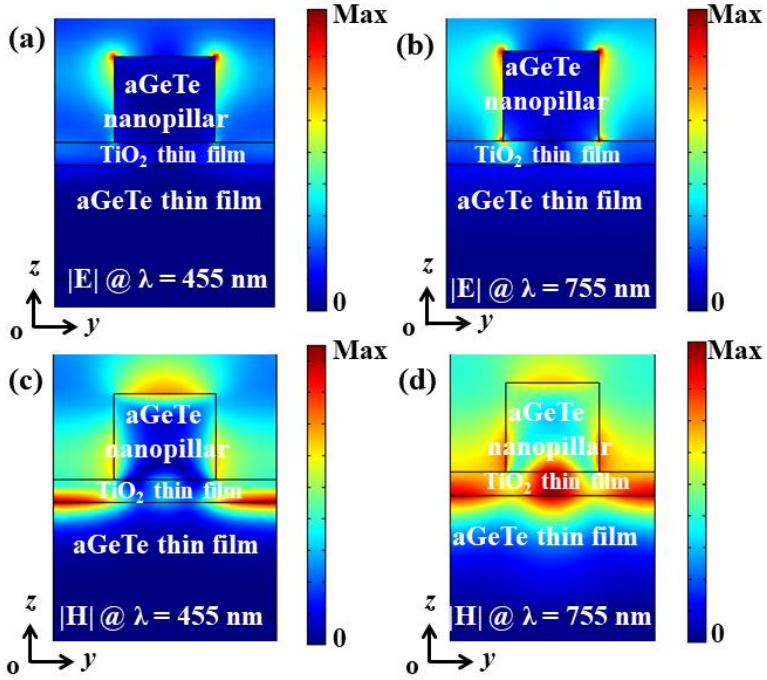

Fig.4 Electromagnetic field distributions of the proposed absorbers at the wavelengths of 455 nm and 755 nm, respectively

Amorphous GeTe thin film can be transformed into crystalline GeTe film by phase-change process induced by optical or electric stimulus. In order to investigate the influence of phase change on broadband absorption performance of the designed absorber, Fig.5 gives the absorption spectra at different phase-change processes. It is noted that the period, radius and height of amorphous GeTe nanopillar are 350 nm, 80 nm and 150 nm, respectively. The thicknesses of middle TiO2 layer and bottom amorphous GeTe thin film are 40 nm and 200 nm, respectively. It can be found that the absorptivity and bandwidth can be freely manipulated via the phase change of top GeTe nanopillar and bottom GeTe film. When the top amorphous GeTe(aGeTe) nanopillar is transformed into its crystalline phase (cGeTe), the absorption peak at 755 nm wavelength is blue-shifted toward 670 nm.When the bottom aGeTe film is further transformed into cGeTe film, the absorptivity at the wavelength of 800~1000 nm is decreased and the absorption bandwidth (absorptivity>90%) becomes narrower.

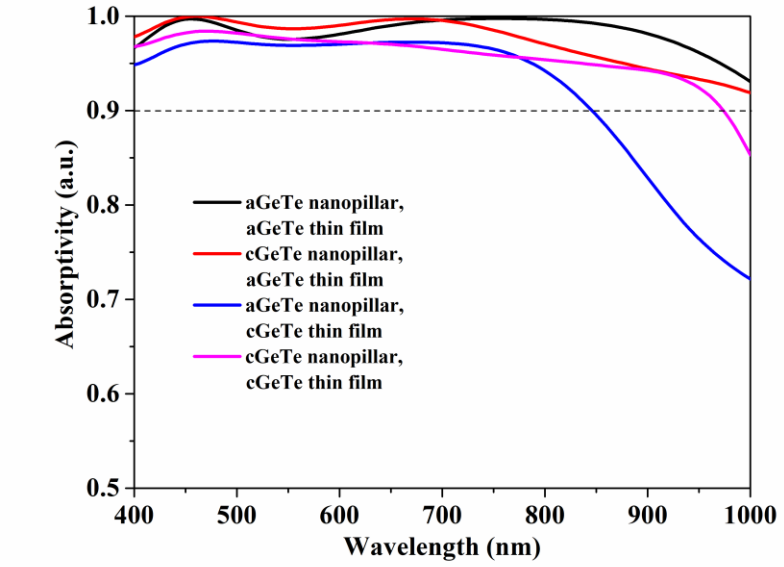

Fig.5 Absorption spectra of the designed absorbers obtained by tuning phase-change process

In order to elucidate the influence of phase-change process on the broadband absorption of the perfect absorber, the electromagnetic field distribution is obtained as shown in Fig.6. Here, the nanopillar is cGeTe material and the absorption peaks are at 460 nm and 670 nm, respectively. It can be seen from Fig.6a and 6b that electric fields are mainly concentrated around the nanopillar at both the wavelengths of 460 and 670 nm. From Fig.6c, the magnetic field is strongest between the TiO2 and aGeTe thin films, leading to the formation of FP resonance.At the wavelength of 670 nm, new magnetic resonance is generated inside the cGeTe nanopillar in addition to the FP resonance as shown in Fig.6d. Thereby, the absorption peak at 755 nm wavelength is blue-shifted toward 670 nm after the phase change from aGeTe nanopillar to cGeTe nanopillar.

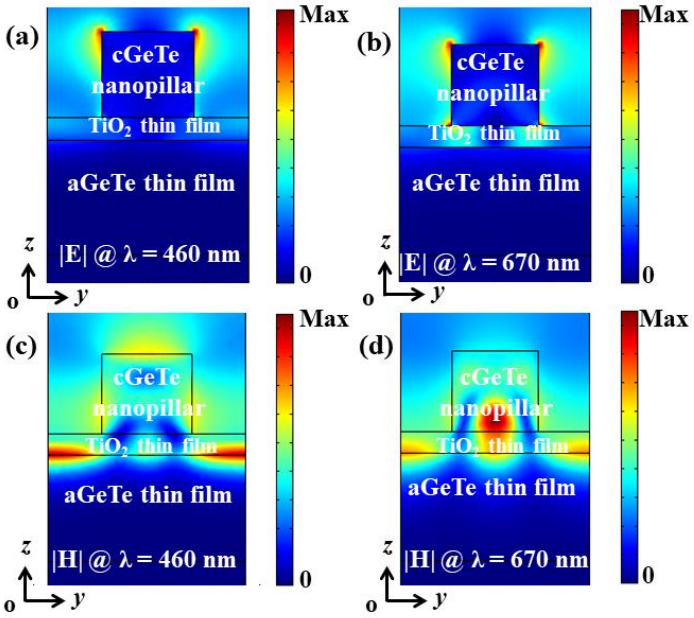

Fig.6 Electromagnetic field distributions of the absorbers after phase change at the wavelengths of 460 nm and 670 nm, respectively.

The perfect absorption performance can be manipulated by changing the thickness of bottom aGeTe thin film. Fig.7 shows the simulated results. Here, the period, radius and height of aGeTe nanopillar are 400 nm, 110 nm and 200 nm, respectively. The thickness of the middle TiO2 layer is 40 nm. It can be seen that the absorptivity gradually increases with the increment of bottom aGeTe thickness in the wavelength range of 400-1000 nm. In parallel, the absorption peak at ~800 nm is red-shifted gradually.

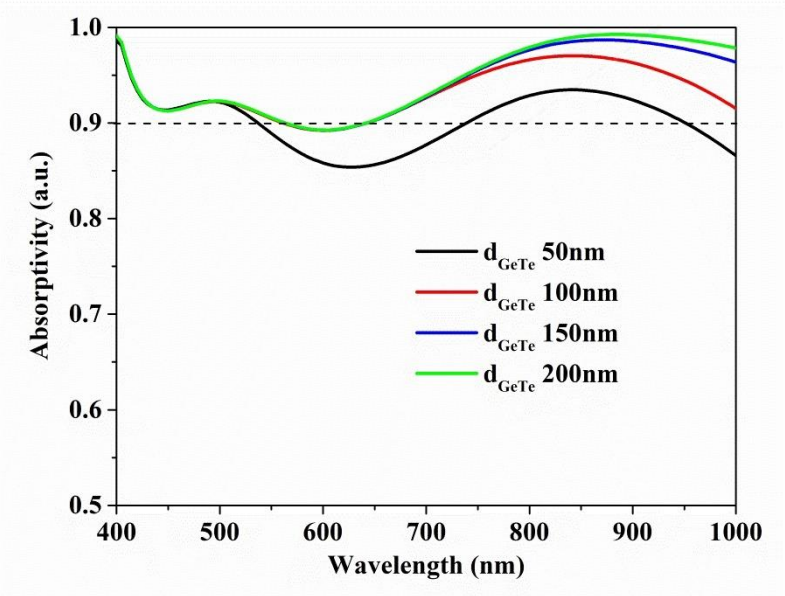

Fig.7 Absorption spectra of the designed absorbers with various thicknesses of amorphousGeTe thin films

In order to explain the above-mentioned phenomenon, Fig.8 shows the electromagnetic field distributions of the absorbers at the absorption peak of 885 nm, where the thickness of aGeTe thin film is 200 nm. One can see electric and magnetic resonances both occur around the aGeTe nanopillar. However, magnetic field is also gathered inside the TiO2 and aGeTe thin films, respectively. Thus, the thickness of aGeTe thin film will influence the magnetic-resonance mode, leading to the shift of absorption peak and intensity.

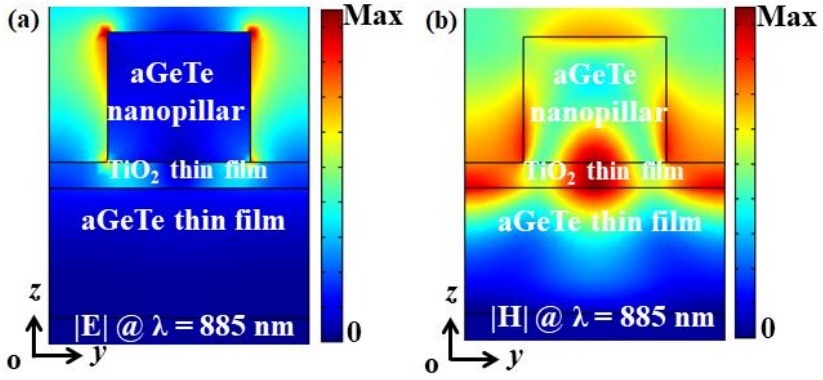

Fig.8 Electromagnetic field distributions of the absorbers at the wavelength of 885 nm

In addition to the bottom aGeTe thin film, the broadband absorption performance may be tuned via changing the thickness of middle TiO2 thin film, top aGeTe radius and height along with the period of nanopillars. Fig.9 shows the absorption spectra of the designed absorbers at various

thicknesses of TiO2 thin films. Here, the period, radius and height of aGeTe nanopillar are 400 nm, 110 nm and 200 nm, respectively. The thickness of the bottom aGeTe layer is 200 nm. One can see that the absorption peak at ~500 nm is red-shifted and the peak at ~800 nm is blue-shifted with the increment of TiO2 thickness. This phenomenon is plausible due to the change of magnetic resonance mode induced by TiO2 thickness, as shown in Fig.4.

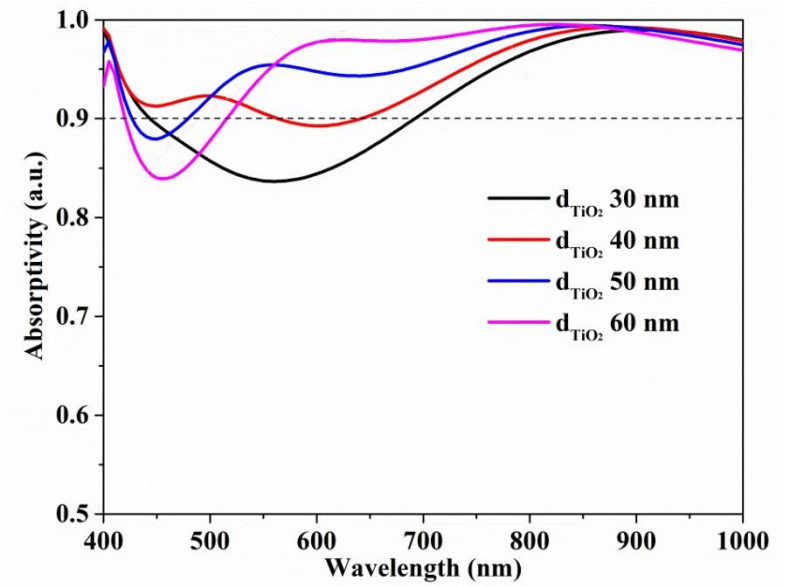

Fig.9 Absorption spectra of the designed absorbers with various thicknesses of TiO2 thin films

Fig. 10 shows the absorption spectra of the designed absorbers with various radiuses of aGeTe nanopillars. Here, the period and height of the top aGeTe nanopillars are 400 nm and 200 nm, respectively. The thicknesses of the middle TiO2 and bottom aGeTe layers are 40 nm and 200 nm, respectively. It is found that the absorptivity at ~500 nm wavelength decreases gradually while the absorptivity at ~900 nm increases with increasing the radius of aGeTe nanopillar. When the radius reaches 80 nm, the absorptivity in the wavelength of 400~1000 nm is higher than 90%. From Fig.4, one can find that the electric and magnetic resonances around the aGeTe nanopillars both influence the broadband absorption performance.

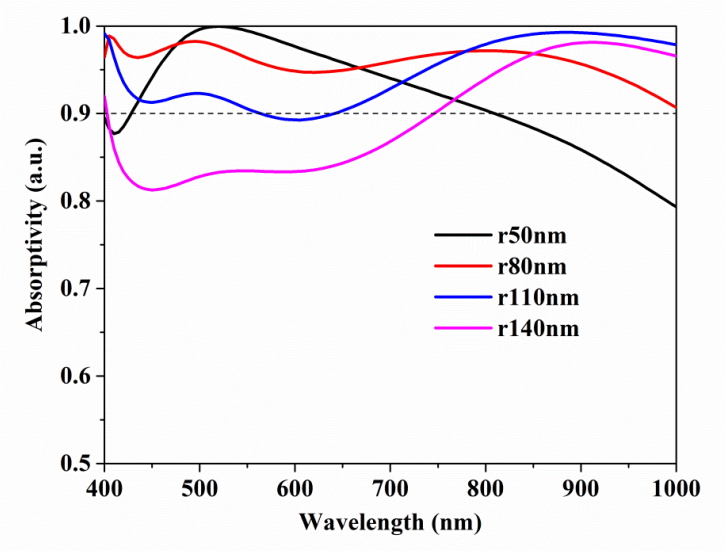

Fig.10 Absorption spectra of the designed absorbers at various radiuses of aGeTe nanopillars

Fig.11 shows the absorption spectra of the absorbers at various heights of aGeTe nanopillars.Here, the period and radius of the top aGeTe nanopillars are 400 nm and 80 nm, respectively. The thicknesses of the middle TiO2 and bottom aGeTe layers are 40 nm and 200 nm, respectively. It can be found that the broadband absorption performance becomes better with increasing the height of nanopillar. However, the absorptivity will reduce slightly when the height is higher 150nm. Therefore, the maximum absorptivity in the wavelength range of 400~1000 nm can be obtained with the nanopillar height of 150 nm.

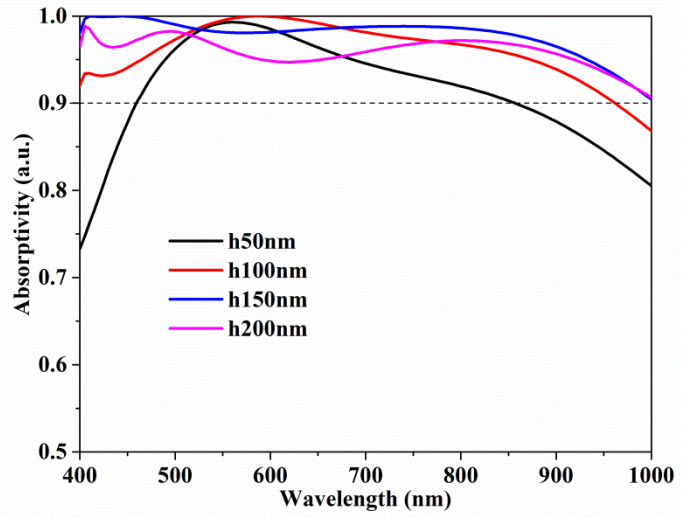

Fig.11 Absorption spectra of the designed absorbers with various heights of amorphous GeTe nanopillar

Fig.12 gives the absorption spectra of the absorbers with various periods of aGeTe nanopillars, where the height and radius of the top aGeTe nanopillars are 150 nm and 80 nm, respectively. The thicknesses of the middle TiO2 and bottom aGeTe layers are 40 nm and 200 nm, respectively. It can be seen that the broadband absorption performance becomes worse when the period of nanopillar reaches 450 nm. The maximum absorptivity (>90%) in 400~1000 nm wavelength can be realized when the period is 350 nm.

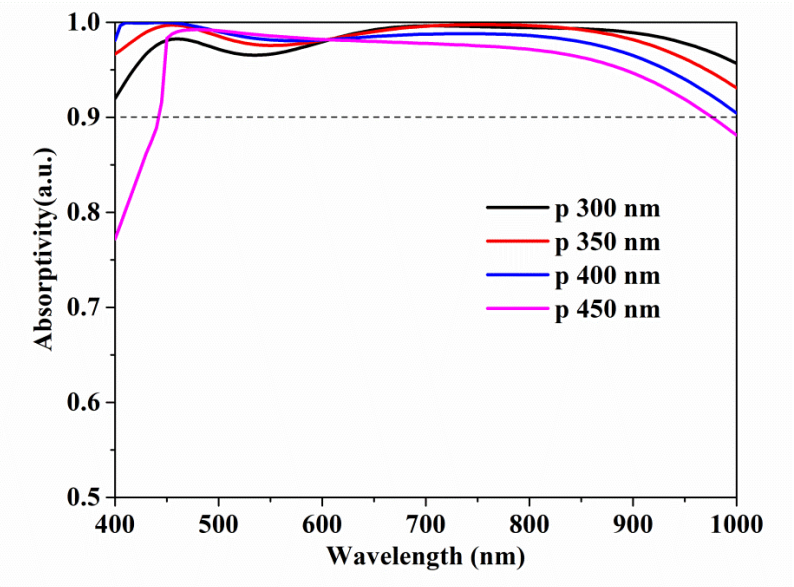

Fig.12 Absorption spectra of the designed absorbers with various periods of amorphous GeTe nanopillar

4. CONCLUSIONS

In summary, a polarization-independent, all-dielectric perfect absorber based on phase-change material has been reported. Broadband (in the wavelength range of 400-1000 nm) absorption of higher than 90% has been realized in our designed absorber. Moreover, absorption bandwidth and absorptivity can be tuned via structural parameters (such as the period, height and radius of nanopillars, the thicknesses of TiO2 and bottom GeTe films) and the phase change from amorphous to crystalline state. The underlying physical mechanism of the absorber is analyzed in detail. The proposed all-dielectric perfect absorber has potential applications in solar energy harvesting.

REFERENCES

1. Qin, F.; Chen, X.; Yi, Z.; Yao, W.; Yang, H.; Tang, Y.; Yi, Y.; Li, H.; Yi, Y., Ultra-broadband and wide-angle perfect solar absorber based on TiN nanodisk and Ti thin film structure. Solar Energy Materials and Solar Cells 2020,211, 110535.
2. Cai, W.; Shalaev, V., Optical Metamaterials--Fundamentals and Applications. Springer Science and Business Media 2010.
3. Jahani, S.; Jacob, Z., All-dielectric metamaterials. Nature nanotechnology 2016,11 (1), 23-36.
4. Cui, T. J.; Smith, D.; Liu, R., Metamaterials: Theory, Design, and Applications. 2010.
5. Padilla, W. J.; Basov, D. N.; Smith, D. R., Negative refractive index metamaterials. Materials Today 2006,9 (7-8), 28-35.
6. Landy, N. I.; Sajuyigbe, S.; Mock, J. J.; Smith, D. R.; Padilla, W. J., Perfect metamaterial absorber. Phys Rev Lett 2008,100 (20), 207402.
7. Zou, C.; Gutruf, P.; Withayachumnankul, W.; Zou, L.; Bhaskaran, M.; Sriram, S.; Fumeaux, C., Nanoscale TiO2 dielectric resonator absorbers. Optics letters 2016,41 (15), 3391-4.
8. Wu, P.; Chen, Z.; Jile, H.; Zhang, C.; Xu, D.; Lv, L., An infrared perfect absorber based on metal-dielectric-metal multi-layer films with nanocircle holes arrays. Results Phys. 2020,16, 102952.
9. Yi, Z.; Liu, L.; Wang, L.; Cen, C.; Chen, X.; Zhou, Z.; Ye, X.; Yi, Y.; Tang, Y.; Yi, Y.; Wu, P., Tunable dual-band perfect absorber consisting of periodic cross-cross monolayer graphene arrays. Results Phys. 2019,13, 102217.
10. Zhang, S.; Wang, Y.; Wang, S.; Zheng, W., Wavelength-tunable perfect absorber based on guided-mode resonances. Appl. Opt. 2016,55 (12), 3176-81.
11. Wang, S.; Chen, F.; Ji, R.; Hou, M.; Yi, F.; Zheng, W.; Zhang, T.; Lu, W., Large-Area Low-Cost Dielectric Perfect Absorber by One-Step Sputtering. Advanced Optical Materials 2019,7 (9), 1801596.
12. Luo, H.; Hu, X.; Qiu, Y.; Zhou, P., Design of a wide-band nearly perfect absorber based on multi-resonance with square patch. Solid State Communications 2014,188, 5-11.
13. Gao, H.; Peng, W.; Liang, Y.; Chu, S.; Yu, L.; Liu, Z.; Zhang, Y., Plasmonic Broadband Perfect Absorber for Visible Light Solar Cells Application. Plasmonics 2019,15 (2), 573-580.
14. Charola, S.; Patel, S. K.; Parmar, J.; Ladumor, M.; Dhasarathan, V., Broadband graphene-based metasurface solar absorber. 2020,62 (3), 1366-1373.
15. Jalil, S. A.; Lai, B.; ElKabbash, M.; Zhang, J.; Garcell, E. M.; Singh, S.; Guo, C., Spectral absorption control of femtosecond laser-treated metals and application in solar-thermal devices. Light Sci Appl 2020,9, 14.
16. Deng, H.; Li, Z.; Stan, L.; Rosenmann, D.; Czaplewski, D.; Gao, J.; Yang, X., Broadband perfect absorber based on one ultrathin layer of refractory metal. Optics letters 2015,40 (11), 2592-5.
17. Luo, M.; Shen, S.; Zhou, L.; Wu, S.; Zhou, Y.; Chen, L., Broadband, wide-angle, and polarization-independent metamaterial absorber for the visible regime. Optics express 2017,25 (14), 16715-16724.
18. Qi, B.; Zhao, Y.; Niu, T.; Mei, Z., Ultra-broadband metamaterial absorber based on all-metal nanostructures. Journal of Physics D: Applied Physics 2019,52 (42), 425304.
19. Hudgens, S.; Johnson, B., Overview of Phase-Change Chalcogenide Nonvolatile Memory Technology. MRS Bulletin 2004,29 (11), 829-832.
20. Dong, W.; Qiu, Y.; Zhou, X.; Banas, A.; Banas, K.; Breese, M. B. H.; Cao, T.; Simpson, R. E., Tunable Mid-Infrared Phase-Change Metasurface. Advanced Optical Materials 2018, 1701346.

21. Du, K.; Cai, L.; Luo, H.; Lu, Y.; Tian, J.; Qu, Y.; Ghosh, P.; Lyu, Y.; Cheng, Z.; Qiu, M.; Li, Q., Wavelength-tunable mid-infrared thermal emitters with a non-volatile phase changing material. Nanoscale 2018,10 (9), 4415-4420.
22. Sreekanth, K. V.; Han, S.; Singh, R., Ge2Sb2Te5-Based Tunable Perfect Absorber Cavity with Phase Singularity at Visible Frequencies. Adv. Mater. 2018,30 (21), 1706696.
23. Cao, T.; Wei, C.-w.; Simpson, R. E.; Zhang, L.; Cryan, M. J., Broadband Polarization-Independent Perfect Absorber Using a Phase-Change Metamaterial at Visible Frequencies. Sci. Rep. 2014,4 (1), 3955.
24. Kats, M. A.; Blanchard, R.; Genevet, P.; Yang, Z.; Qazilbash, M. M.; Basov, D. N.; Ramanathan, S.; Capasso, F., Thermal tuning of mid-infrared plasmonic antenna arrays using a phase change material. Optics letters 2013,38 (3), 368-370.
25. Wang, J.; Li, Q.; Tao, S.; Xia, Z.; Li, Y.; Liu, Y.; Gu, Z.; Hu, C., Improving the reflectance and color contrasts of phase-change materials by vacancy reduction for optical-storage and display applications. Opt. Lett. 2020,45 (1), 244-247.
26. Rasheed, M.; Barillé, R., Optical constants of DC sputtering derived ITO, TiO2 and TiO2:Nb thin films characterized by spectrophotometry and spectroscopic ellipsometry for optoelectronic devices. J. Non-Cryst. Solids 2017,476, 1-14.
27. Jafari, M.; Guo, L. J.; Rais-Zadeh, M., A Reconfigurable Color Reflector by Selective Phase Change of GeTe in a Multilayer Structure. Advanced Optical Materials 2019,7 (5), 1801214.
28. Devlin, R. C.; Khorasaninejad, M.; Chen, W. T.; Oh, J.; Capasso, F., Broadband high-efficiency dielectric metasurfaces for the visible spectrum. Proceedings of the National Academy of Sciences of the United States of America 2016,113 (38), 10473-8.
29. Mou, N.; Liu, X.; Wei, T.; Dong, H.; He, Q.; Zhou, L.; Zhang, Y.; Zhang, L.; Sun, S., Large-scale, low-cost, broadband and tunable perfect optical absorber based on phase-change material. Nanoscale 2020,12, 5374-5379.